Journal of Metals, Materials and Minerals, Vol. 29, No. 4, pp. 99-105, 2019

Failure analysis of superheat tube 2.25Cr-1Mo in biomass power plant

Boonhlua KHWANSRI[1], Mai NOIPITAK[2,*], and Viboon TANGWARODOMNUKUN[1]

[1] *Department of Production Engineering, Faculty of Engineering, King Mongkut's University of Technology Thonburi, 126 Pracha Uthit Rd., Bang Mod, Thung Khru, Bangkok 10140, Thailand*
[2] *Materials and Nondestructive Testing Laboratory, King Mongkut's University of Technology Thonburi (Ratchaburi), Rang Bua, Chom Bueng, Ratchaburi 70150, Thailand*

[*]**Corresponding author e-mail:** mai.noi@kmutt.ac.th

Received date:
8 October 2018
Revised date:
30 April 2019
Accepted date:
12 May 2019

Keywords:
Biomass power plant
Erosion
Failure
Superheat tube

Abstract

The understanding of microstructures, their influences, and failure mechanisms are of necessary for determining lifetime and failure behaviors of metal parts being used in some severe environments. This research aims to study the failure causes and mechanisms of superheat tube used in a power plant. The tube examined in this experiment was 2.25Cr-1Mo (SA213 Grade T22) with a diameter of 33.5 mm and 4.33-mm wall thickness. This tube had been in-service for 7.5 years in a 9.9-MW biomass power plant. Visual inspection, chemical analysis with an optical emission spectrometer, optical microstructure, scanning electron microscope (SEM), energy dispersive X-ray (EDS), hardness measurement and tensile were employed to investigate the causes of superheat tube failure. The results showed that the damaged tube was subjected to the non-uniform loss of outer wall thickness due to erosion and presence of ferrous oxide at the outer tube surface. The hardness of outer and inner tube surfaces was found to be less than that of the mid-wall section. In addition, carbide particles were observable and uniformly dispersed throughout the microstructures. Regarding the SEM result, the tube failure was relevant to the bursting with ductile fracture.

1. Introduction

Boiler is used for steam producing to spin turbines and convert their rotational energy into electricity. The steam temperature can be up to 540°C with the internal pressure of 10-100 bar. With this high temperature and pressure, materials used for making the boiler and its associated equipment have to be able to withstand such severe condition and also maintain their mechanical strength for a sufficiently long service life. A superheat tube used in the steam boiler is a seamless type and it is made of alloy steels such as Cr-Mo [1,2,3] which is able to maintain the tube strength at elevated temperature. However, the service life of the tube is highly dependent on the operating condition of the boiler. The actual service life is usually shorter than the maximum design limit due to some uncontrollable factors induced while using the boiler. A precise estimation of the part's service life can be attained by investigating the failure modes as well as the changes of metallurgical and mechanical properties of the work material. Information gained from these analyses can facilitate a better prediction of part deterioration and time to failure.

The 2.25Cr-1Mo (SA213-T22) and 9Cr-1Mo-V (SA213-T91) alloy steels have commonly been used in high-temperature refinery, petrochemical and power plants due to their high creep, and high corrosion resistance. After operating in various conditions with a long period of time, some tube properties could be changed and lead to failure accordingly. The determination of temperature changes and oxide scale thickness during its services can estimate the remaining life of the superheat tube. The failure mechanism can be classified into two types; i.e. expected and unexpected ones. The expected mechanism is about creep, fatigue, and corrosion, while the unexpected failure is relevant to internal-thermal shock cracking. The latter mechanism is usually difficult to be inspected as well as to form a proper preventive maintenance program [4].

The failures of superheat tube have been investigated by many researchers through the different mechanisms such as overheating, oxidation, stress rupture, stress corrosion cracking, creep [5], thermal fatigue, ash/high temperature corrosion [6,7] and erosion [8,9]. Goutam Das et al [10] noted that a failed 2.25Cr-1Mo tube taken from a coal power plant is caused by carbide precipitate in its grain boundary and inside the grain. Srikanth et al [11] stated that the root cause of boiler tube failure is fire side corrosion and hydrate ferric sulphate formation. Sodium, sulfur and vanadium elements in tube materials can result in a scale formation and a reduction of tube thickness. These elements also cause the coagulation of carbides on the outer and inner surfaces of tube utilized under a long term overheating.

For the internal corrosion of boiler tube, a water treatment program such as phosphate treatment, caustic treatment and amine treatment can be applied to prevent and reduce the corrosion to the inner tube surface. Oxides formed on the internal surface can cause poor heat transfer efficiency across the tube surface and also increase the fuel consumption of boiler system. This adversely leads to the undesirable temperature rising in the component, and in turn

DOI: 10.14456/jmmm.2019.52

induces the localized heating, formation of coarsened carbides and precipitation of brittle phases. These effects promote the embrittlement of the tube and creep void formation along the grain boundary as well as the presence of high hoop stress [12]. In addition, the scale depositing in a boiler system potentially increases the fuel consumption. A caustic corrosion in a low alloy steel (SA-210 Grade A-1) can be evidenced at the waterline of a partially filled tube. Phosphate treatment is thereby applied to prevent the corrosion through the reduction of soft particle calcium and magnesium formation in boiler water [13].

Ahmad [14] investigated a failed T22 tube welded with Incoloy 800 and found that graphitization and decarburization are the causes of failure. Purbolaksono et al [15] investigated a damaged SA213-T12 tube by using visual inspection, hardness measurement, and finite element analysis. The localized overheating induced by flue gas flow is a primary cause of failure. Thermal fatigue and corrosion fatigue are the causes of failure in boiler tube grade SA210-A1. Ahmad et al [16] reported that the side wall tube is mainly damaged by the thermal fatigue, while other sections are failed by a combination of corrosion fatigue, thermal fatigue and creep. Ahmad [17] additionally investigated a SA213-T22 tube, which had been in-service for 17 years with an overheating condition, and found the spheroidization of carbide particles in the micro-structure. These results clearly demonstrate the effects of overheating on the tube failure.

The failure analysis of a superheat tube grade SA213-T22 was undertaken in this study. The tube had been used for approximately 50,000 hours in a biomass power plant, in which the flue gas from the biomass combustion passed through and attacked the tube in horizontal. A diagram of the boiler is shown in Figure 1, and a tube sample was taken for examination. Corrosion, erosion and other possible causes of failure defined by the aid of visual inspection and micro-structural analysis were accounted in this study. The findings of this research could provide the essential information for monitoring and evaluating the condition, service life and failure mechanisms of the superheat tube used in the biomass power plant and other similar environments.

2. Experimental

A superheat tube specimen was ASTM A213 grade T22 having the outside diameter of 33.5 mm and thickness of 4.33 mm as shown in Figure 2. The tube has been attacked by flue gas during the year 2008 to 2015. The biomass power plant has been operated again in early 2017, and an operator found a tube leakage in June 2017. Thus, the tube is anticipated to be in-service for 7.5 years. Rice husk and chopped wood were used for combustion and generating the flue gas. The combustion temperature in the chamber was about 750-950°C. The flue gas flowing from the combustion chamber to the superheat tube was controlled to be not greater than 850°C for heating at an intermediate temperature vapor range of 200-300°C up to a high temperature vapor of 480°C at the pressure of 68-73 bar. The specimen was cross sectioned and examined by visual inspection, measurement of chemical composition, optical microstructure, scanning electron microscope (SEM), energy dispersive X-ray (EDS), micro-hardness, and tensile testing.

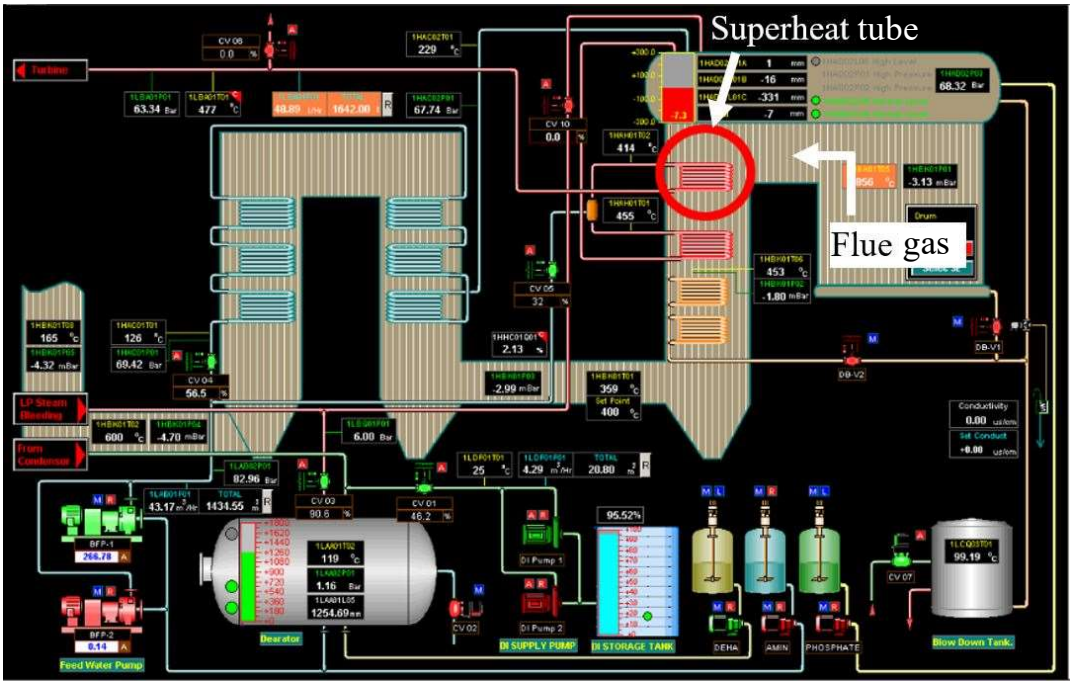

Figure 1. Location of failed tube in a biomass power plant.

Figure 2. A sample cut from a failed superheat tube (a) overview, (b) cross section of tube.

The visual inspection and tube dimensions were conducted by using an ultrasonic thickness measurement (UTM). The chemical composition was measured and analyzed by using an Optical Emission Spectrometer (ARL-3460, Therno Fisher, Germany). The samples were prepared by the sand wheel grinding of tube wall to get a sufficiently large-flat surface for the spectrometer. To observe the microstructures of the tube sample, the specimen was polished and etched in 2% nital solution according to ASTM E04 [21] before being observed by an optical microscope (Axio vert 200M, Zeiss, Germany) with regard to ASTM E1382. A scanning electron microscope (SEM) (JSM-IT300, JEOL, USA) equipped with energy dispersive X-ray (EDS) (X-MAX [IE-350], OXFORD, USA) was also employed to provide a higher image resolution for the micrograph analysis.

Vickers hardness measurement was carried out by Wilson hardness testing machine (432 SDV, Instron, USA) under a 10-kgf load and the dwell time of 10 seconds according to ASTM E92-17 standard [18]. The maximum hardness of original material was about 163 BHN (~170 VHN), which corresponds to the suggested value for SA213-T22 steel [19]. The hardness value was also converted to the ultimate tensile strength (UTS) by using [10,20].

$$\text{Ultimate tensile strength } (\sigma, \text{MPa}) \approx 3.4 \times \text{BHN} \quad (1)$$

The failed tube hardness was 154.7 BHN (~162 VHN) and it can be converted to the UTS of 525 MPa, while the UTS of the original tube was around 554.2 MPa. The tensile strength was measured by a tensile testing machine (1000 HDX, Intron, USA) with the tensile speed of 5 mm·min^{-1} according to ASTM D370-2017 [21].

3. Results and discussion

3.1 Visual inspection

As shown in Figure 2, damages are apparent on the external tube surface especially at the fireside whose wall thickness was found to be less than 2.5 times the opposite side (Figure 3). This is a result of flue gas impingement at the temperature of around 850°C. The particles of rice husk and chopped wood mixing with the flue gas scratched the external tube surface, commonly known as fly-ash erosion, and this finding is similar to the studies of Das [22] and Pronobis [23]. The fly ash erosion with the different impinging angles is anticipated to cause the non-uniform tube thickness. Erosion is usually occurred in the biomass boiler. The increased amount of ash particles in the flue gas stream can decrease the thickness of boiler tube and in turn leads to a rupture. The increase in particle velocity exponentially increases the erosion rate. Moreover, the impinging angle, size and shape of the particles play a vital role in the surface erosion [24,25]. The erosion rate substantially increases when the particle size of larger than 30 μm strikes the surface. The large amount of solid particles in the gas typically increases the erosion rate, but this effect may be imperceptible when the amount of particles is of very high [26]. Furthermore, the severe erosion is evidenced when the particle size is equal to 1000 μm [27].

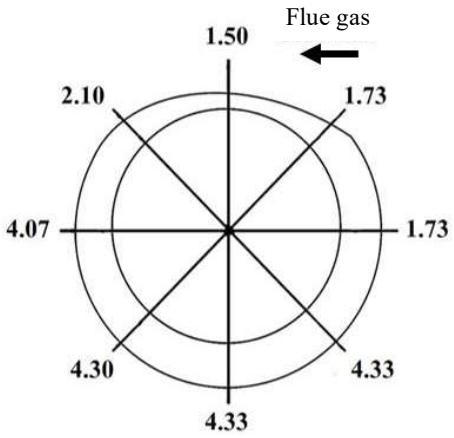

Figure 3. Wall thickness of failed tube (unit in mm).

The greatest erosion occurs when using non-spherical particles with sharp edges and high hardness. The maximum tube erosion is apparent at the impinging angle of approximately 40 degrees to the axis of the flue gas stream [28]. According to the sample, the wall thickness was reduced approximately by 74% on the fireside, where it was attacked at the high temperature of flue gas and fly ash particles. In addition, the tube burst was found in the longitudinal direction.

3.2 Chemical composition and microstructures

The chemical analysis was performed by using the spectroscopy, and the chemical composition of thin and thick sides were compared to ASTM A213 Grade T22 as listed in Table 1. The measurement indicated no significant difference of chemical composition on the both sides respecting to the T22 grade.

The external fireside was cut and ground as shown in Figure 4.

The specimens of virgin and damaged tubes were cross sectioned, mounted and polished as shown in Figure 5 for microstructural analysis. The micrographs of virgin and damaged tubes are shown in Figure 6 and 7, respectively. The virgin tube composed of ferrite grains (white area) and nodules of pearlite structures (dark area), while the failed tube was subjected to phase transformations. As mentioned in the Figure 7, the heated tube was in recovery status. The stored internal energy was relieved, as a result of enhanced atomic diffusion at the elevated temperature. After recovery was complete, the grains are still in a relatively high strain energy state. The new set of strain-free and equiaxed grains were formed, known as recrystal-lization process. The driving force to produce this new grain structure is the difference in internal energy between the strained and unstrained material. The new grains form as very small nuclei and grow until they completely consume the parent material [29].

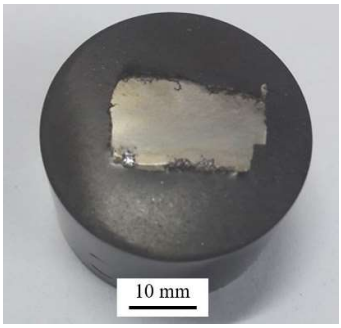

Figure 4. Overview of surface specimen.

Table 1. Chemical composition of work sample.

Element	Composition (%)						
	C	Mn	P	S	Si	Cr	Mo
Thin side	0.12	0.47	0.01	0.02	0.30	2.01	0.89
Thick side	0.11	0.47	0.01	0.01	0.30	2.06	0.90
A213 Gr. T22	0.05-0.15	0.30-0.60	0.025	0.025	0.50	1.90-2.60	0.87-1.13

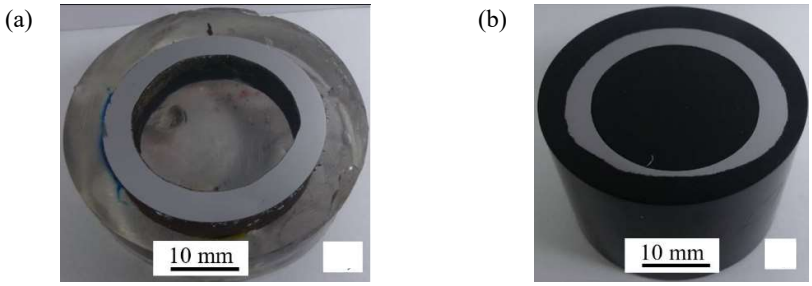

Figure 5. Specimens of (a) virgin tube and (b) damaged tube.

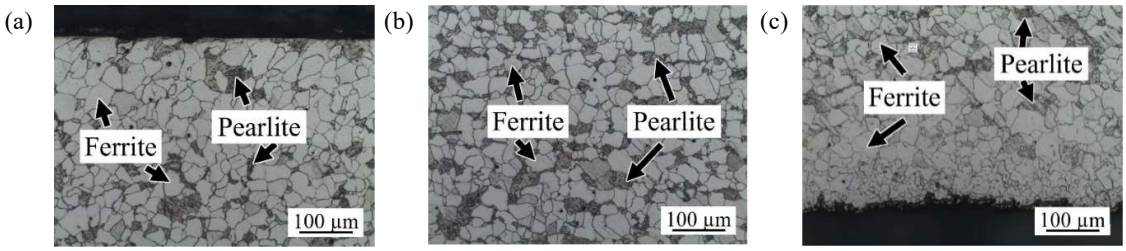

Figure 6. Microstructures of virgin tube (a) outside (b) mid-wall (c) inside.

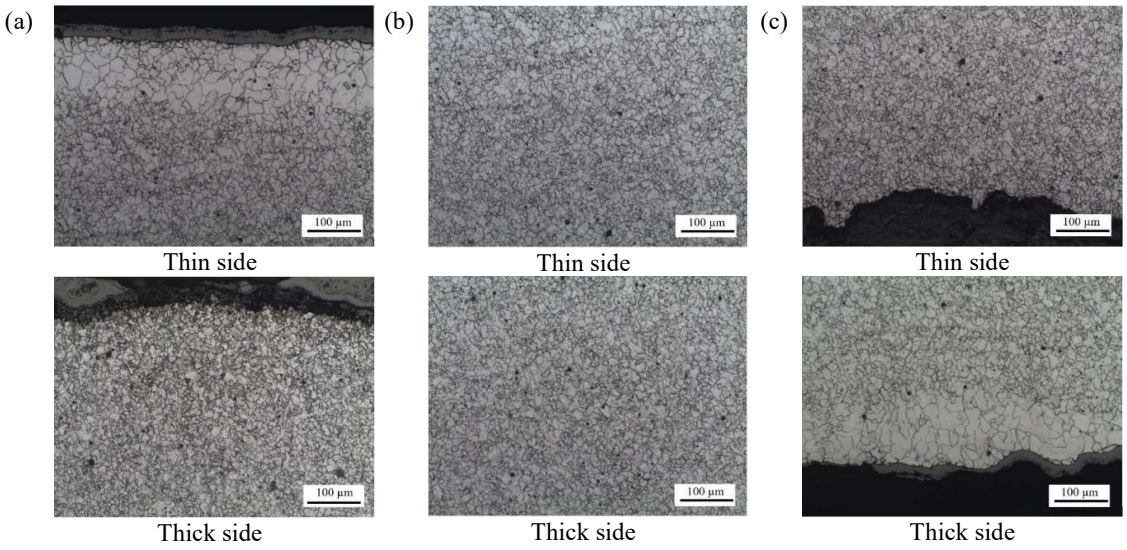

Figure 7. Microstructures of failed tube (a) outside (b) mid-wall (c) inside.

3.3 Micro hardness and tensile strength

The micro-hardness was performed on the thin side (fireside) and compared to the average hardness of the virgin tube. The hardness was measured from the inner surface (steam side) to the outer surface (fireside) with the total of 10 points. The results shown in Figure 8 indicated that the average micro-hardness of the virgin tube was 170 HV (~163 HBN max), while the minimum and maximum values of hardness at the inner surface were 125.6 HV and 171.5 HV, respectively. The hardness was found to reduce both on fire side and steam side due to the long time heating. The hardness of steam side was lower than the fireside due to the small amount of coagulated carbides. The hardness reduction of failed tube could also be a consequence of the microstructural changes; i.e. formation of new grain particle, dissolution of pearlite and carbide formation [30].

At operating condition, the hoop stress of superheat tube can be calculated by using:

$$\sigma H = \frac{Pr}{t} \quad (2)$$

where σH, P, r and t are hoop stress, pressure, tube radius and tube wall thickness, respectively. The maximum pressure during the operating temperature of 480°C was around 73 bar. Then, the calculated hoop stress was 22.8 MPa, indicating the safety factor of about 9 since the minimum yield strength of SA213-T22 at room temperature is 205 MPa [31]. However, the boiler was operated at the temperature of around 480°C. At this temperature, the yield strength of SA213-T22 decreases to 96.18 MPa [30], thus making the safety factor of only 2. This reduction of safety factor cannot allow the tube to withstand the internal pressure during its service for a long period of operation. The tensile stress of damaged tube was performed and its yield strength was 340 MPa. At the operating temperature of 480°C, the yield strength is 96.18 MPa, so that the minimum tube thickness (t) is 1.36 mm. When the temperature increases to 580°C, the estimated yield strength is 32.3 MPa and the minimum wall thickness required has to be 3.56 mm.

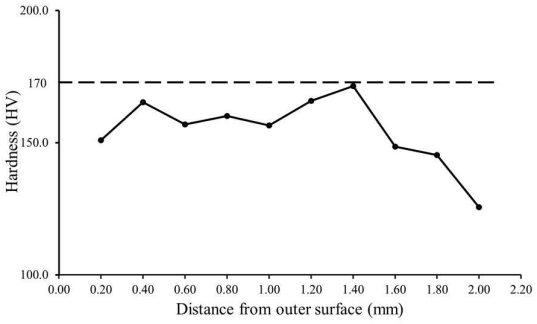

Figure 8. Micro-hardness at different distances from the inner surface.

3.4 SEM&EDS

The characteristic of damage area was investigated by using SEM. From the SEM result shown in Figure 9, the microstructure at the burst region was stretched associated with ductile tube fracture.

The external fireside was investigated. A high magnification image taken by SEM is presented in Figure 10, demonstrating the new grain particles (indicated by arrows) and carbides at the grain boundaries.

The EDS results are shown in figure 11. The first zone of tested area (spectrum 1) shown the normal element of 2.25Cr-1Mo steel. Oxygen content approximately 3.84 percent by weight was detected and Cr element was found due to the formation of Cr-Mo

steel. In contrast, the second zone of tested area (spectrum 2) was found that the composition of the 2.25Cr-1Mo steel remained while oxygen content increased to 45.77 percent by weight. The experimental results reveal the corrosion region occurred with dissolved oxygen and the dark area could be ferrous oxides which similar to the report of Ahmed [17].

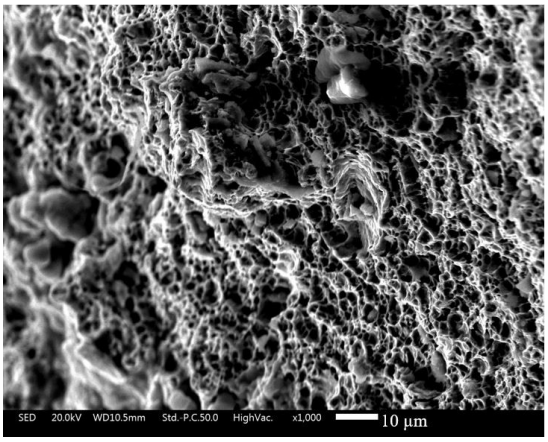

Figure 9. SEM micrograph of damage region.

(a)

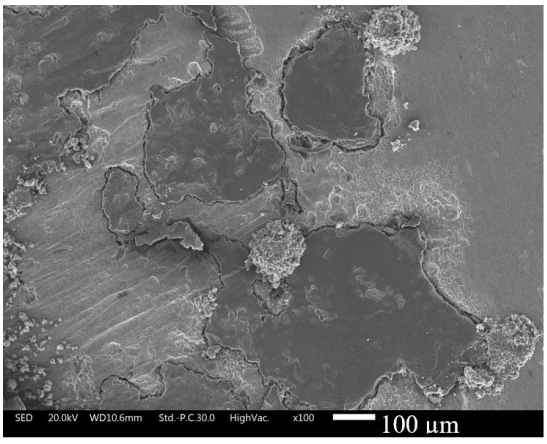

(b)

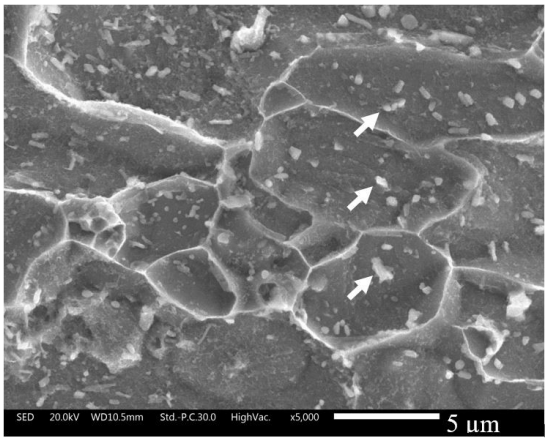

Figure 10. SEM micrograph of external surface (a) corrosion area, (b) grain boundary.

4. Conclusions

A damaged SA213 Grade T22 superheat tube taken from a biomass power plant was investigated in this study to determine the root cause of failure. The corrosion was found on the fireside of the tube, and its wall thickness was thinner than the steam side due to the fly ash erosion. The hardness of fireside was higher than that of steam side. However, the tensile strength of superheat tube was found to be in accordance with the material specification. The SEM result at the burst region of damaged tube showed the ductile fracture. The increased chromium in the microstructure caused the grain nucleation and some migrations to the grain boundary in the form of chromium carbide. According to all findings, the microstructural changes and fly ash erosion were the root causes of the superheat tube failure examined in this study.

5. Acknowledgements

The authors would like to thank Mr. Damri Santatiwongchai and staffs of UWC Komen Biomass Co., Ltd. for providing the tube sample as well as information to be analyzed in this research.

References

[1] H. Abbasfard, M. Ghanbari, A. Ghasemi, S. Ghader, H. H. Rafsanjani, and A. Moradi, "Failure analysis and modeling of super heater tubes of a waste heat boiler thermally coupled in ammonia oxidation reactor," *Engineering Failure Analysis*, vol. 26, pp. 285-292, 2012.

[2] S. Xu, C. Wang, and W. Wang, "Failure analysis of stress corrosion cracking in heat exchanger tubes during start-up operation," *Engineering Failure Analysis*, vol. 51, pp. 1-8, 2015.

[3] Damage mechanisms affecting fixed equipment in the refining industry. API 571;2003: 4.35 and 4.95.

[4] J. Salonen, P. Auerkari, O. Lehtinen, and M. Pihkakoski, "Experience on in-service damage in power plant components," *Engineering Failure Analysis*, vol. 14, pp. 970-977, 2007.

[5] D. R. H. Jones, "Creep failures of overheated boiler, superheater and reformer tubes," *Engineering Failure Analysis*, vol.11, pp. 873-893, 2004.

[6] A. I. Almazroueea, K. J. Al-Fadhalah, S. N. Alhajeria, and S.Alfehaidc, "High temperature corrosion of martensitic steel of reheater pipes in a desalination power plant," *Engineering Failure Analysis*, vol. 85, pp. 89-96, 2018.

[7] K. K. Parthiban, "Chorline induced high temperature superheater corrosion in biomass power plants," *Venus Energy Audit System.*

[8] McGraw-Hill, *Nalco Guide to Boiler Failure Analysis,* second ed., Nalco company, 2011.

[9] F. J. Chen, C. Yao, and Z. G. Yang, "Failure analysis on abnormal wall thinning of heat-transfer titanium tubes of condensers in nuclear power plant part II: Erosion and cavitation corrosion," *Engineering Failure Analysis*, vol. 37, pp. 42-52, 2014.

[10] G. Das, S. G. Chowdhury, A. K. Ray, S. Das, and D. K. Bhattacharaya, "Failure of a super heater tube," *Engineering Failure Analysis*, vol. 9, pp. 563-570, 2002.

[11] S. Srikantha, B. Ravikumarb, S. K. Dasb, K. Gopalakrishnaa, K. Nandakumarc, and P. Vijayanc, "Analysis of failures in boiler tubes due to fireside corrosion in a waste heat recovery boiler," *Engineering Failure Analysis*, vol. 10, pp. 59-66, 2003.

[12] A. K. Pramanick, G. Das, S. K. Das, and M. Ghosh, "Failure investigation of super heater tubes of coal fired power plant," *Case studies in Engineering Failure Analysis*, vol. 9, pp. 17-26, 2017.

[13] F. Daneshvar-Fatah, A. Mostafaei, R. Hosseinzadeh-Taghani, and F. Nasirpouri, "Caustic corrosion in a boiler waterside tube: Root cause and mechanism," *Engineering Failure Analysis,* vol. 28, pp. 69-77, 2013.

[14] J. Ahmad and J. Purbolaksono, "An incident investigation on stub tube at high temperature reheater outlet header region of a power plant," *Engineering Failure Analysis*, vol. 17, pp. 1254-1259, 2010.

[15] J. Purbolaksono, J. Ahmad, L. C. Beng, A. Z. Rashid, A. Khinani, and A. A. Ali, "Failure analysis on a primary superheater tube of a power plant," *Engineering Failure Analysis*, vol. 17, pp. 158-167, 2010.

[16] J. Ahmad, J. Purbolaksono, and L. C. Beng, "Thermal fatigue and corrosion fatigue in heat recovery area wall side tubes," *Engineering Failure Analysis*, vol. 17, pp. 334-343, 2010.

[17] J. Ahmad and J. Purbolaksono, "Analysis on a failed 2.25Cr–1Mo reheater bent tube at upper bank vertical tubes region," *Engineering Failure Analysis,* vol. 18, pp. 523-529, 2011.

[18] V. Meuronen, "Ash particle erosion on steam boiler convective section," *Lappeenranta University of Technology*. Research Papers 64, Lappeenranta, 1997.

[19] L. Zhang, V. Sazonov, J. Kent, T. Dixon, and V. Novozhilov, "Analysis of boiler-tube erosion by the technique of acoustic emission: Part I. Mechanical erosion," *Wear*, vol. 250, Issues 1-12, pp. 762-769, 2001.

[20] G. I. Parslow, D. J. Stephenson, J. E. Strutt JE, and S. Tetlow, "Paint layer erosion resistance behavior for use in a multilayer paint erosion indication technique," *Wear,* vol. 212, pp. 103-9, 1997.

[21] G. Heiermann, H. Langner, C. Brinkmann, and H. Mondry, "Konstruktionskriterien zur erosions-minderung in wirbelschichtfeuerungen. wirbel-schichtfeuerung und Dampferzeugung," *Essen*, 1988.

[22] M. Pronobis, "Modernisation of power boilers" *(Modernizacja kotłów energetycznych) WNT Warsaw*, 2002.

[23] ASTM E92-2017, *Standard Test Method for Vickers Hardness of Metallic Materials*, 2017.

[24] ASTM A213 T22 *Alloy steel seamless tube.*

[25] G. E. Dieter, *Mechanical metallurgy*, SI metric edition. McGraw Hill Book Company, pp. 331, 1988.

[26] ASTM A370 Standard Test Methods and Definitions for Mechanical Testing of Steel Products, 2017.

[27] S. K. Das, K. M. Godiwalla, S. P. Mehrotra, K. K. M. Sastry, and P. K. Dey, "Analytical model for erosion behavior of impacted fly-ash particles on coal-fired boiler components," *Sadhana*, vol. 31, pp. 583-595, 2006.

[28] M. Pronobis and W. Wojnar, "The impact of biomass co-combustion on the erosion of boiler," *Energy Conversion and Management*, vol. 74, pp. 462-470, 2013.

[29] W. D. Callister and Jr. D. G. Rethwisch, Callister, *Material science and engineering an introduction*. USA: John Wiley & Sons, Inc., 1940.

[30] B. M. Jenkins, L. L. Baxter, T. R. Miles Jr., and T. R. Miles, "Combustion properties of biomass," *Fuel Processing Technology*, vol. 54, pp. 17-46, 1998.

[31] ASME Section II, Part D, 2007